Local structure at the manganese site in mixed-valence manganites

G. Subías, J. García,* J. Blasco, and M. G. Proietti
Instituto de Ciencia de Materiales de Aragón, CSIC-Universidad de Zaragoza, Facultad de Ciencias, Plaza San Francisco, 50009-Zaragoza, Spain
(Received 9 July 1997)

Extended x-ray absorption fine structure at the manganese *K* edge has been used to study the first oxygen coordination shell at the manganese site as a function of temperature in mixed-valence perovskites. $La_{1-x}Ca_xMnO_3$ ($x=0$, 0.15, 0.33, 0.5, 0.66, and 1), $La_{0.60}Y_{0.07}Ca_{1/3}MnO_3$, $La_{0.57}Tb_{0.1}Ca_{1/3}MnO_3$, and $Tb_{1-x}Ca_xMnO_3$ ($x=0$, 0.33, 0.5, and 0.67) were studied. Our results show that the manganese atom is surrounded by a regular oxygen octahedra in the metallic-ferromagnetic phase. The analysis of the spectra at temperatures above the magnetic transition can be described in terms of either a unique Mn-O interatomic distance with a large Debye-Waller factor or two Mn-O distances with a distortion lower than 0.1 Å. Such distortion or disorder must be dynamic since it cannot be detected by diffraction measurements. This result supports the evidence of a large phonon-electronic interaction and the polaronic origin as a possible mechanism of electrical conduction in the paramagnetic phase. [S0163-1829(98)03101-4]

I. INTRODUCTION

The physical properties of manganese oxides $RE_{1-x}A_xMnO_3$ (RE=La,Pr,..; A=Ca,Sr,Ba) are now being investigated due to the discovery of colossal magnetoresistance effects associated with the ferromagnetic-paramagnetic phase transition. A great experimental and theoretical effort is currently being devoted to understand the intriguing behavior of these kinds of compounds.[1–12]

The series $La_{1-x}Ca_xMnO_3$ can be considered as an archetype of these kinds of materials. The phase diagram can be described briefly as follows:[13] $LaMnO_3$ orders antiferromagnetically at 140 K showing weak ferromagnetism due to spin canting.[14] This low-temperature ordered state is present in the $La_{1-x}Ca_xMnO_3$ series up to $x=0.1$. In the composition range between $0.1<x<0.5$ the system orders ferromagnetically when cooling down, coupled to a large decrease in the electrical resistivity, i.e., a metal-insulator (MI) phase transition. Simultaneous metallic state and ferromagnetic ordering was explained by the double exchange model proposed by Zener and developed by Anderson and De Gennes.[15–17] When x is larger than 0.5, the manganese sublattice orders antiferromagnetically and a charge ordering (CO) state is developed.[18–20] These features have been traditionally explained as due to the competition between superexchange antiferromagnetic interactions of Mn(III)-O-Mn(III) and Mn(IV)-O-Mn(IV) on the one hand, and the ferromagnetic double exchange interaction of Mn(III)-O-Mn(IV) on the other.

Recently, several studies have shown a strong electron-phonon coupling at both the MI phase transition and the CO transition.[5,19,20] The importance of the lattice dynamics in the mechanism of the electronic and magnetic transitions has suggested different possible models that include the presence of lattice polarons of the Janh-Teller (JT) type.[8,10,19,21,22] This means a local JT distortion due to the splitting of the outer Mn^{3+} 3*d* level. Up to now there is no evidence about the existence of local distortions induced by JT coupling in the paramagnetic phase. X-ray and neutron-diffraction techniques have shown small distortion,[23–25] typically an order of magnitude lower than those observed for static or dynamic JT distortions.[26] Previous works on extended x-ray-absorption fine structure (EXAFS) spectroscopy at the manganese *K* edge have reported different results for these materials. Tyson *et al.*[27] observed a single-site Mn-O bond length distribution below T_c, while a multisite distribution was observed above T_c. Booth *et al.*[28] have observed only a discontinuous change of the Debye-Waller factor at the phase transition with a unique Mn-O bond distance. Moreover, negligible changes are observed in x-ray absorption near-edge structure (XANES) spectra[29] across the phase transition indicating no modifications of the local structure, in agreement with the results of Booth *et al.*[28]

The local structure determination and, in particular, the possible relationship between local vibrational modes and electron motion is very important to understand the behavior of these materials. The oxygen arrangement in the MnO_6 octahedra should be determined in order to test the JT polaronic model proposed by several authors.[8,10,19,21,22] In a recent work we have studied these materials with different compositions, with the presence of a magnetic field and at different temperatures by means of XANES and circular magnetic x-ray dichroism (CMXD) techniques at the Mn *K* edge.[28] Our results have shown only one kind of manganese atom independently of the formal Mn^{3+}/Mn^{4+} ratio, i.e., a pure mixed-valence state with a fluctuation time lower than 10^{-19} sec. In order to account for this problem we have investigated the local structure by EXAFS spectroscopy at the manganese *K* edge in an extensive number of samples according to the following points: (i) study of the variation of the local structure as a function of the composition in the $La_{1-x}Ca_xMnO_3$ series; (ii) study of the structural changes in the ferromagnetic and paramagnetic phases of $(La_{1-x}RE_x)_{2/3}Ca_{1/3}MnO_3$; (iii) study of the local structure of $Tb_{1-x}Ca_xMnO_3$ series that does not show ferromagnetic ordering.

TABLE I. Lattice parameters at room temperature (Å), magnetic and electrical transition temperatures (K), and references. T_N denotes the Neel temperature, T_C the Curie temperature, T_{CO} the CO transition temperature, T_{MI} the MI transition temperature, SC indicates a semiconducting behavior, and SG a spin-glass behavior at low temperatures.

	Unit cell			Physical properties		
Sample	*a*	*b*	*c*	Magnetic	Electrical	Reference
$LaMnO_3$	5.535	5.723	7.697	$T_N=140$	SC	12, 19
$La_{0.85}Ca_{0.15}MnO_3$	5.501	5.536	7.737	$T_C=180$	$T_{MI}\approx T_C$	6, 19
$La_{2/3}Ca_{1/3}MnO_3$	5.472	5.457	7.711	$T_C=260$	$T_{MI}\approx T_C$	19, 23
$La_{1/2}Ca_{1/2}MnO_3$	5.470	5.433	7.688	$T_C=230$	$T_{MI}\approx T_C$	19
				$T_N=195$	$T_{CO}\approx T_N$	
$La_{1/3}Ca_{2/3}MnO_3$	5.404	5.379	7.580	$T_N=160$	$T_{CO}=275$	19, 20
$CaMnO_3$	5.268	5.281	7.458	$T_N=120$	SC	19, 30
$La_{0.6}Y_{0.07}Ca_{1/3}MnO_3$	5.455	5.455	7.697	$T_C=160$	$T_{MI}\approx T_C$	5
$La_{0.57}Tb_{0.1}Ca_{1/3}MnO_3$	5.452	5.454	7.693	$T_C=150$	$T_{MI}\approx T_C$	23
$TbMnO_3$	5.301	5.854	7.399	$T_N=15$	SC	30
$Tb_{2/3}Ca_{1/3}MnO_3$	5.326	5.529	7.496	$SG+T_N=70$	SC	30
$Tb_{1/2}Ca_{1/2}MnO_3$	5.337	5.462	7.472	$T_N=140$	$T_{CO}=300$	30
$Tb_{1/3}Ca_{2/3}MnO_3$	5.312	5.376	7.485	$T_N=130$	$T_{CO}=285$	30

II. EXPERIMENTAL DETAILS

Samples were synthesized using a sol-gel method by the citrate route. The synthetic route and physical characterization have been reported elsewhere.[5,7,17,23,30] The samples were characterized by means of x-ray-powder diffraction as single-phase materials with an orthorhombic perovskite structure. Oxygen content was tested by titration redox using $KMnO_4$ and Mohr's salt. The main magnetic, crystallographic, and transport properties of the studied samples are summarized in Table I.

The experiments were performed at three different synchrotron radiation facilities, beam line 18 at ESRF (Grenoble); beam line 7.1 at SRS (Daresbury), and beam line XAS 4 at LURE (Orsay). Identical EXAFS spectra were obtained for samples measured at the three facilities. Spectra were recorded in transmission mode using a fixed exit beam double Si(111) crystal monochromator. The energy resolution $\Delta E/E$ was estimated to be about 2×10^{-4} for all of the measurements. Harmonic rejection was achieved by a slight detuning of the two crystals from the parallel alignment. Silicon photodiodes were used to detect the incident and transmitted flux at ESRF while ionization chambers were used at

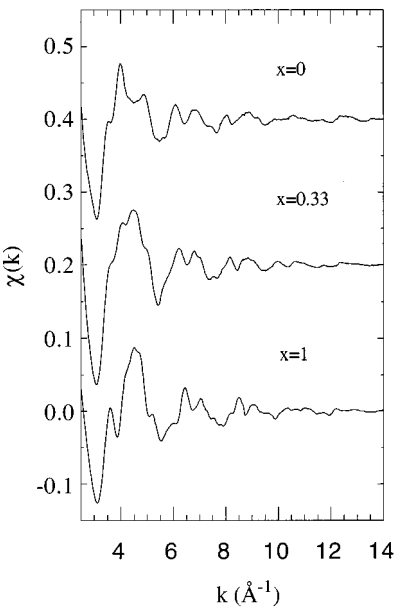

FIG. 1. Room temperature manganese *K* edge EXAFS spectra of $La_{1-x}Ca_xMnO_3$ ($x=0.0.33,1$).

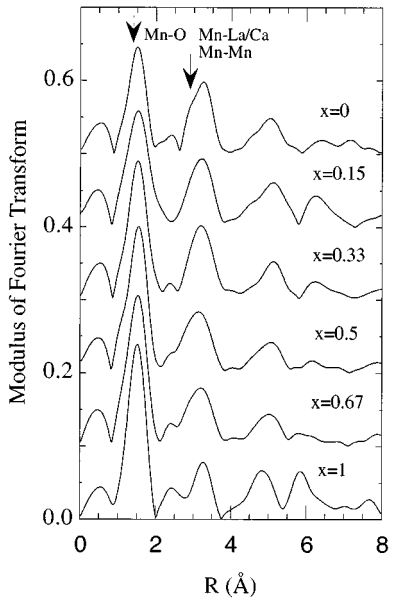

FIG. 2. Modulus of the Fourier transform of the EXAFS spectra of $La_{1-x}Ca_xMnO_3$ series at room temperature. Data have been transformed between 3.5 and 14 $Å^{-1}$ using a Gaussian window.

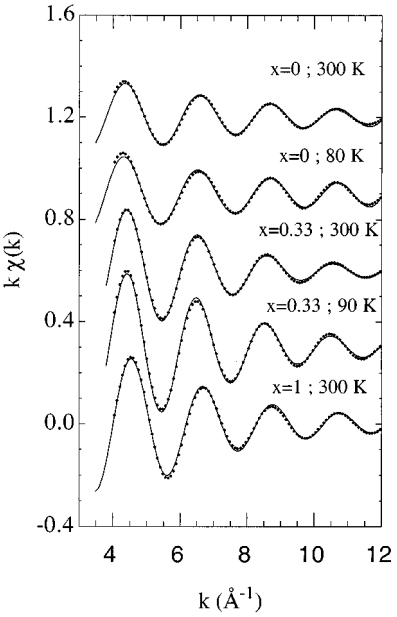

FIG. 3. Comparison between Fourier filtered first shell experimental spectra and best-fit simulations of $La_{1-x}Ca_xMnO_3$ ($x=0,0.33,1$) samples at different temperatures. An only Mn-O distance has been considered for $x=0.33$ sample.

LURE and SRS. Cryostats were used for recording the spectra at low temperatures and the temperature control was regulated within 0.1 K in all cases, but the sample temperature could be as much as 2 K higher than the nominal temperature.

The structural analysis has been reduced to the first oxygen shell because it is the most relevant parameter in order to understand the possible mechanism conducting the behavior of these systems. Data were reduced following standard procedures.[31] The EXAFS signals were extracted from the raw spectra measured in a wide range (800 eV above the edge). The background subtraction was performed by means of a cubic spline that simulates the monotonic atomic absorption coefficient (μ_0), therefore the EXAFS signal was obtained as $\chi(k)=[\mu(k)-\mu_0(k)]/\mu_0(k)$, where k is the magnitude of the photoelectron wave vector obtained as $k=[2m(E-E_0)]^{1/2}/\hbar$, being E_0 the $1s$ binding energy determined by the inflection point of the experimental spectra. The first shell contribution was extracted by Fourier filtering (FF) of the spectra between 1 and 2 Å. The structural parameters were obtained by least-square fitting of the filtered spectra using as reference the first shell signal of $CaMnO_3$. EXAFS of this sample was also analyzed using the theoretical phases and amplitudes generated from the FEFF 3.11 code.[32]

TABLE II. Results of the structural analysis of the first oxygen coordination shell of $La_{1-x}Ca_xMnO_3$ EXAFS spectra at the Mn K edge as a function of temperature. N is the coordination number, R and $\langle R\rangle$ are the interatomic and the average Mn-O distances, respectively, $\Delta\sigma^2$ is the Debye-Waller factor for the Mn-O distance referred to the value for the $CaMnO_3$ sample, σ^2 is the absolute value for the Debye-Waller factor and Res. is the best-fit residual factor normalized for ν, i.e., the difference between the number of independent points of the spectra and the number of fit parameters (Ref. 33). Estimated errors for Mn-O bonds are ± 0.01. EXAFS data are compared with x-ray-diffraction (XRD) data.

			XRD	EXAFS				
Sample	T (K)	N	R (Å)	R (Å)	$\langle R\rangle$ (Å)	$\Delta\sigma^2$ (Å^2) $\times 10^{-3}$	σ^2 (Å^2) $\times 10^{-3}$	Res.
$LaMnO_3$	RT	4	1.94	1.94		−0.2	1.3	0.01
		2	2.17	2.21		8.5	10	
	20 K	4	1.94	1.94		−1.7	0.0	0.01
		2	2.16	2.18		3.8	5.3	
$La_{0.85}Ca_{0.15}MnO_3$	RT	6		1.96		3.3	4.8	0.001
		4		1.93	1.98	−0.3	1.2	0.002
		2		2.06		−0.2	1.3	
	120 K	6		1.96		2.1	3.6	0.003
		4		1.94	1.98	−0.7	0.8	0.005
		2		2.05		−1.0	0.4	
$La_{0.67}Ca_{0.33}MnO_3$	RT	6	1.96	1.94		1.4	2.9	0.001
		4		1.92	1.95	−0.15	1.3	0.003
		2		2.00		0.1	1.6	
	240 K	6		1.95		−0.1	1.4	0.002
	90 K	6		1.96		−1.8	0.0	0.003
$La_{0.5}Ca_{0.5}MnO_3$	RT	6		1.94		0.7	2.2	0.002
$La_{0.33}Ca_{0.67}MnO_3$	RT	6		1.93		0.5	2.0	0.002
$CaMnO_3$	RT	6	1.90	1.92		0.0	1.5	0.002

III. RESULTS

A. EXAFS spectra of the series $La_{1-x}Ca_xMnO_3$ ($x=0$, 0.15, 0.33, 0.5, 0.66, and 1)

Figure 1 shows the EXAFS spectra for $LaMnO_3$, $La_{2/3}Ca_{1/3}MnO_3$, and $CaMnO_3$ samples. The spectra are highly structurated indicating the crystalline character of the samples. The Fourier transform of the room temperature spectra taken between 3.5 and 14 $Å^{-1}$ are shown in Fig. 2. We observe a main peak ascribed to the first oxygen shell and further peaks, corresponding to successive coordination shells. The intensity of the first peak for $LaMnO_3$ is lower than for the other samples, making evident the presence of a tetragonal distortion.

Comparisons between experimental spectrum and the best-fit simulation are shown for $CaMnO_3$, $LaMnO_3$, and $La_{2/3}Ca_{2/3}MnO_3$ in Fig. 3. The best-fit parameters are summarized in Table II. Only one best fit was obtained for all the samples at room temperature except for $La_{0.85}Ca_{0.15}MnO_3$ and $La_{2/3}Ca_{1/3}MnO_3$. In these samples two different best fits are obtained with very small differences between the accuracy factors. The two solutions are, either well a nondistorted MnO_6 octahedron with an only Mn-O bond length with a large Debye-Waller factor, or a MnO_6 octahedron with two Mn-O distances and low Debye-Waller factors. Although, the one-shell fit seems to be better on a statistical point of view, i.e., in terms of the residual factor reported in Table II. Both fits are in agreement with a large spread of the interatomic distances above T_c. It is important to note that coor-

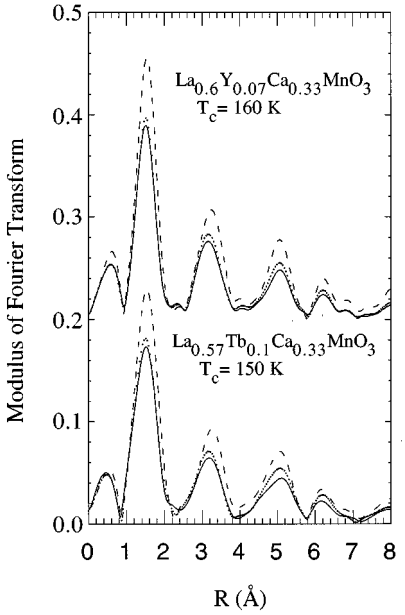

FIG. 4. Fourier transform of the EXAFS spectra for $(La_{1-y}RE_y)_{2/3}Ca_{1/3}MnO_3$ samples at temperatures above and below the MI phase transition. Solid lines represent the room-temperature data. Pointed curves are data taken at 180 K. Dashed lines are data taken at 80 K for the Y sample and 105 K for the Tb sample.

TABLE III. Results of the structural analysis of the first oxygen coordination shell of $(La_{1-y}RE_y)_{2/3}Ca_{1/3}MnO_3$ series with RE = Y or Tb as a function of temperature. Fit parameters are the same as those defined in Table II. Estimated errors for Mn-O bonds are ± 0.01. EXAFS data are compared with XRD data.

			XRD	EXAFS				
Sample	T (K)	N	R (Å)	R (Å)	$\langle R\rangle$ (Å)	$\Delta\sigma^2$ (Å^2) $\times 10^{-3}$	σ^2 (Å^2) $\times 10^{-3}$	Res.
$La_{0.67}Ca_{0.33}MnO_3$	RT	6	1.96	1.94		1.4	2.9	0.001
		4		1.92	1.95	−0.1	1.4	0.003
		2		2.00		0.1	1.6	
	240 K	6		1.95		−0.1	1.4	0.002
	90 K	6		1.96		−1.8	0.0	0.003
$La_{0.6}Y_{0.07}Ca_{0.33}MnO_3$	RT	6	2×1.97	1.95		2.1	3.6	0.001
			2×1.96					
		4	2×1.95	1.93	1.96	−0.8	0.7	0.002
		2		2.03		0.4	2.0	
	180 K	6		1.94		1.7	3.2	0.001
		4		1.92	1.95	−0.8	0.7	0.002
		2		2.02		0.6	2.2	
	80 K	6	1.96	1.96		−1.1	0.4	0.003
$La_{0.57}Tb_{0.1}Ca_{0.33}MnO_3$	RT	6	1.96	1.95		2.7	4.2	0.002
		4		1.92	1.96	0.0	1.5	0.004
		2		2.03		0.0	1.6	
	180 K	6		1.94		2.2	3.7	0.001
		4		1.92	1.95	−0.3	1.2	0.003
		2		2.02		−0.4	1.1	
	105 K	6		1.96		−0.3	1.2	0.002
	20 K	6		1.96		−0.9	0.6	0.003

TABLE IV. Results of the structural analysis of the first oxygen coordination shell of $Tb_{1-x}Ca_xMnO_3$ EXAFS spectra at the Mn *K* edge as a function of temperature. Fit parameters are the same as those defined in Table II. Estimated errors for Mn-O bond are ± 0.01. EXAFS data are compared with XRD data.

			XRD	EXAFS				
Sample	T (K)	N	R (Å)	R (Å)	$\langle R \rangle$ (Å)	$\Delta\sigma^2$ (Å^2) $\times 10^{-3}$	σ^2 (Å^2) $\times 10^{-3}$	Res.
			2×1.88					
$TbMnO_3$	RT	4	2×1.93	193		−0.3	1.2	0.009
		2	2×2.28	2.29		9.1	11	
	20 K	4		1.92		−1.0	0.5	0.002
		2		2.26		4.0	5.5	
			2×1.96					
$Tb_{0.67}Ca_{0.33}MnO_3$	RT	4	2×1.95	1.92	1.96	0.4	1.9	0.002
		2	2×2.01	2.05		11	12.2	
	20 K	4		1.92		−0.2	1.3	0.003
		2		2.03		0.6	2.1	
$Tb_{0.5}Ca_{0.5}MnO_3$	320 K	6	1.95	1.94		2.3	3.8	0.002
$Tb_{0.33}Ca_{0.67}MnO_3$	RT	6		1.94		0.6	2.2	0.001
$CaMnO_3$	RT	6	1.90	1.92		0.0	1.5	0.002

dination numbers have been fixed in the fit process. The difference between the bond lengths, obtained by the two-shell fit, ranges between 0.08 and 0.1 Å, very similar to the Debye-Waller factor values (0.05–0.07 Å) obtained in the fit with an only distance. Samples with $x=0.5$ and $x=\frac{2}{3}$ only show an interatomic distance with low Debye-Waller factors. The interatomic Mn-O distances are in nice agreement with the distances obtained from diffraction measurements as can be seen in Table II and show a monotonic decrease with increasing x, due to the increase of the average manganese valence state.

B. Series $(La_{1-x}RE_x)_{2/3}Ca_{1/3}MnO_3$

The effect of the so-called ''chemical pressure,'' i.e., the decrease of the radius of the A atom (r_A) in ABO_3 perovskites obtained in this case by substitution of lanthanum with smaller rare-earth atoms, induces a decrease in the temperature of both, the MI and magnetic phase transitions. In order to characterize the MnO_6 octahedra in the paramagnetic phase for different r_A values, we have performed EXAFS experiments in two different samples, $La_{0.6}Y_{0.07}Ca_{0.33}MnO_3$ and $La_{0.57}Tb_{0.1}Ca_{0.33}MnO_3$. The Fourier transform of the spectra taken at temperatures above and below the phase transition are shown in Fig. 4. The intensity of the peak ascribed to the Mn-O distance increases, as expected, with decreasing the temperature, but the change is much more evident across the MI transition temperature, independently of the absolute value of T_c. This means that the Mn-O bond-length disorder is strongly reduced when the MI transition takes place. Analysis of the first shell was performed using $CaMnO_3$ as reference and the best-fit values are given in Table III. As in the case of $La_{2/3}Ca_{1/3}MnO_3$ an only interatomic distance is obtained for the samples with long-range ferromagnetic ordering. Nevertheless, the paramagnetic region can be described again by a large Debye-Waller factor or a local distortion. We want to emphasize that the accuracy of both fits are similar and, consequently, the technique cannot distinguish between the two possibilities.

C. Series $Tb_{1-x}Ca_xMnO_3$

$Tb_{1-x}Ca_xMnO_3$ series does not show long-range ferromagnetism for any composition.[30] Therefore, its study allows us to distinguish the effects of the rare-earth substitution with Ca from the effects arising from ferromagnetic ordering. The results of the first shell analysis are reported in Table IV. First shell data for $TbMnO_3$ show two interatomic distances characteristic of a JT splitting as occurs for $LaMnO_3$. The distortion for $TbMnO_3$ is larger than for $LaMnO_3$, in part due to the smaller ionic radius of the Tb atom. $Tb_{2/3}Ca_{1/3}MnO_3$ shows a small distortion at room temperature and at 20 K in agreement with the x-ray-diffraction studies. In this case, the fit using a local distortion is clearly better than the fit obtained by using a unique distance, in contrast with the results obtained for $La_{2/3}Ca_{1/3}MnO_3$ and RE substituted samples. Samples with $x=\frac{1}{2}$ and $x=\frac{1}{3}$ show a unique Mn-O interatomic distance in agreement with crystallographic studies.

The first shell filtered spectra at high and low temperatures of the homologous compounds $La_{1/3}Ca_{2/3}MnO_3$ and $Tb_{2/3}Ca_{1/3}MnO_3$ are compared in Fig. 5. It allows us to visualize the absence of distortion in the ferromagnetic phase, i.e., the interference between two different interatomic distances that gives rise to a lower signal for the distorted spectra. On the other hand, the high-temperature phase of $Tb_{2/3}Ca_{1/3}MnO_3$ is more distorted than its homologous $La_{2/3}Ca_{1/3}MnO_3$ sample.

IV. DISCUSSION AND CONCLUSIONS

The extensive EXAFS study performed has allowed us to determine the local structure of three different series of manganite compounds and, in particular, the short-range order at the Mn site above and below the MI phase transition in the magnetoresistive lanthanum-calcium based manganese perovskites. Several points can be considered for discussion. The first point is the evidence of regular MnO_6 octahedra in the metallic ferromagnetic phase independent of the phase transition temperature of the compound considered. Our re-

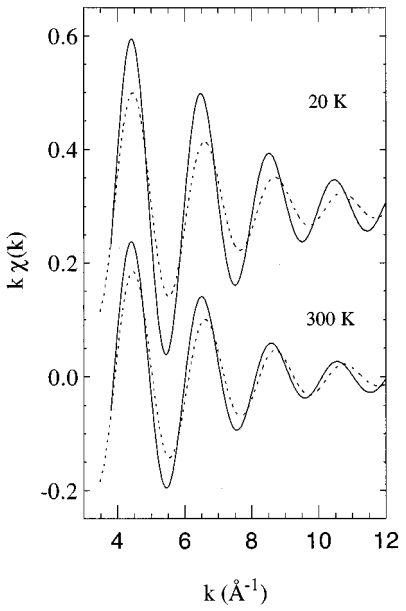

FIG. 5. Comparison of the first shell EXAFS contribution of the isoelectronic $La_{2/3}Ca_{1/3}MnO_3$ (continuous line) and $Tb_{2/3}Ca_{1/3}MnO_3$ (dashed line) samples at room and low temperatures.

sults agree with diffraction results obtained by several authors[5,6,19,23,24] and complete previous EXAFS experiments.[27,28,34] This point, around which some consensus is growing within the scientific community, puts in evidence that if the MI transition is driven by coupling with phonons, such a coupling does not stabilize any kind of local distortion in the ferromagnetic phase. This result, together with recent XANES and CMXD results, points to the presence of a unique kind of manganese atom in the ferromagnetic phase, therefore Mn is shown to be in a pure mixed-valence state. These results points out that the ferromagnetic metallic state would be better described in the framework of band theory models and as it has been suggested by Picket and Singh,[9] as a half-metallic ferromagnet.

Second, our results clearly show the presence of an anomalous structural disorder of the MnO_6 octahedra in the paramagnetic phase for the magnetoresistive materials. Our opinion about some of the controversies found in the literature about the EXAFS results for this phase is that they can arise from the intrinsic limitations of the EXAFS technique. In fact, our analysis gives a similar agreement by considering a unique Mn-O distance or two distances. This fact is consistent with the typical resolution of distances achievable by EXAFS that is determined by the useful k range data.[35] In our case, i.e., with a k range of about 10 $Å^{-1}$, differences in distances lower than 0.15 Å cannot be unambiguously resolved. In any case, the large Debye-Waller factors obtained in the former case allow us to conclude that paramagnetic phase is characterized by a large random static or dynamic disorder. Either the Debye-Waller factor or the distortion obtained by the two-shell fit are lower than the static distortion found in the homologous $Tb_{2/3}Ca_{1/3}MnO_3$ or in $LaMnO_3$ and $TbMnO_3$ where the distortion is originated by the splitting of the e_g ground state. This point together with the absence of any kind of distortion obtained by diffraction studies,[5,6,19,23,24] suggests a dynamic distortion that collapses at the phase transition. Moreover, it is impossible to distinguish from EXAFS results the driving force of the distortion, i.e., between a breathing mode and a JT distortion. Our results can support the mechanism of polaronic conduction above T_c as it has been suggested by magnetostriction and small-angle neutron-scattering results.[11] This result also agrees with theoretical studies that propose a localization of the conduction-band electrons as polarons by electron-phonon coupling and below T_c the polaron effect is turned off allowing the formation of a metallic state.

Furthermore, $Tb_{2/3}Ca_{1/3}MnO_3$ shows features similar to the isoelectronic $La_{2/3}Ca_{1/3}MnO_3$ at room temperature but the local distortion remains for the Tb compound at low temperatures where long-range ferromagnetism no longer takes place. This point indicates that the phase transition has a magnetic origin, being the decrease of local Mn-O disorder a consequence of the ferromagnetic coupling of the manganese atoms.

Regarding nonmagnetoresistive perovskites, i.e., for $x > 0.5$, our results coincide with the diffraction results, giving interatomic distances arising from the average value of the oxidation state and Debye-Waller factor values lower than those found at room temperature in the magnetoresistive materials. We would like also to emphasize that from a structural point of view a unique manganese is detected, which means no disproportion of Mn atoms.

ACKNOWLEDGMENTS

We would like to thank Dr. A. Filipponi and Dr. P. Loeffen of ESRF, Dr. D. Bazin and H. Sonneville of LURE, and K. C. Cheung of SRS for technical assistance at the respective facilities. The authors are grateful to the EC Large Facilities Program, ESRF, and the Spanish DGICYT for financial support (Project No. MAT96-0491).

*Corresponding author. Tel:+34-76-761225; Fax: +34-76-761229; Electronic address: jgr@posta.unizar.es

[1] R. von Helmholt, J. Wecker, B. Holzapfel, L. Shultz, and K. Samwer, Phys. Rev. Lett. **71**, 2331 (1993).

[2] S. Jin, T. H. Tiefel, M. McCormack, R. A. Fastnacht, R. Ramesh, and L. H. Chen, Science **264**, 413 (1994).

[3] A. Asamitsu, Y. Morimoto, Y. Tomioka, T. Arima, and Y. Tokura, Nature (London) **373**, 407 (1995).

[4] G. Zhao, K. Conder, H. Keller, and K. A. Muller, Nature (London) **381**, 770 (1996).

[5] M. R. Ibarra, P. A. Algarebel, C. Marquina, J. Blasco, and J. García, Phys. Rev. Lett. **75**, 3541 (1995).

[6] H. Y. Hwang, S. W. Cheong, P. G. Radaelli, M. Marezio, and B. Batlogg, Phys. Rev. Lett. **75**, 914 (1995).

[7] J. M. de Teresa, M. R. Ibarra, J. García, J. Blasco, C. Ritter, P. A. Algarabel, C. Marquina, and A. del Moral, Phys. Rev. Lett. **76**, 3392 (1996).

[8] A. J. Millis, P. B. Littlewood, and B. I. Shraiman, Phys. Rev. Lett. **74**, 5144 (1995).

[9] W. E. Pickett and D. J. Singh, Phys. Rev. B **53**, 1146 (1996).

[10] H. Röder, J. Zang, and A. R. Bishop, Phys. Rev. Lett. **76**, 1356 (1996).

[11] J. M. de Teresa, M. R. Ibarra, P. A. Algarabel, C. Ritter, C. Marquina, J. Blasco, J. García, A. del Moral, and Z. Arnold, Nature (London) **386**, 256 (1997).
[12] C. Ritter, M. R. Ibarra, J. M. de Teresa, P. A. Algarabel, C. Marquina, J. Blasco, S. Oseroff, and S. W. Cheong, Phys. Rev. B **56**, 8902 (1997).
[13] P. Schiffer, A. P. Ramirez, W. Bao, and S. W. Cheong, Phys. Rev. Lett. **75**, 3336 (1995).
[14] G. Matsumoto, J. Phys. Soc. Jpn. **29**, 606 (1970).
[15] C. Zener, Phys. Rev. **82**, 403 (1951).
[16] P. W. Anderson and H. Hasegawa, Phys. Rev. **100**, 675 (1955).
[17] P. G. de Gennes, Phys. Rev. **118**, 141 (1960).
[18] A. P. Ramirez, P. Schiffer, S. W. Cheong, C. H. Chen, W. Bao, T. T. M. Palstra, P. L. Gammet, D. J. Bishop, and B. Zegarsky, Phys. Rev. Lett. **76**, 3188 (1996).
[19] P. G. Radaelli, M. Marezio, H. Y. Hwang, S. W. Cheong, and B. Batlogg, Phys. Rev. Lett. **75**, 4488 (1995).
[20] M. R. Ibarra, J. M. de Teresa, J. Blasco, P. A. Algarabel, C. Marquina, J. García, J. Stankiewicz, and C. Ritter, Phys. Rev. B **56**, 8252 (1997).
[21] A. J. Millis, B. I. Shraiman, and R. Mueller, Phys. Rev. Lett. **77**, 175 (1996).
[22] J. S. Zhou, W. Archibald, and J. B. Goodenough, Nature (London) **381**, 770 (1996).
[23] J. Blasco, J. García, J. M. de Teresa, M. R. Ibarra, P. A. Algarabel, and C. Marquina, J. Phys.: Condens. Matter **8**, 7427 (1996).
[24] J. L. García-Muñoz, M. Suaaidi, J. Fontcuberta, and J. Rodriguez-Carvajal, Phys. Rev. B **55**, 34 (1997).
[25] Z. Jiràk, S. Krupicka, Z. Simsa, M. Dlohuhá, S. Vratislav, J. Magn. Magn. Mater. **53**, 153 (1985).
[26] S. Gota, J. García, J. Chaboy, and J. Bartolomé, Phys. Rev. B **44**, 11 632 (1991).
[27] T. A. Tyson, J. Mustre de León, S. D. Conradson, A. R. Bishop, J. J. Neumeier, and J. D. Thompson, Phys. Rev. B **53**, 13 985 (1996).
[28] C. H. Booth, F. Bridges, G. J. Synder, and T. H. Geballe, Phys. Rev. B **54**, R15 606 (1996).
[29] G. Subías, J. García, M. G. Proietti, and J. Blasco, Phys. Rev. B **56**, 8183 (1997).
[30] J. Blasco, J. García, J. M. de Teresa, M. R. Ibarra, J. Pérez, P. A. Algarabel, C. Marquina, and C. Ritter, Phys. Rev. B **55**, 8905 (1997).
[31] *X-ray Absorption Techniques of EXAFS, SEXAFS and XANES*, edited by D. C. Koningsberger and R. Prins (Wiley, New York, 1988).
[32] J. J. Rehr, J. Mustre de León, S. I. Zabinsky, and R. C. Albers, J. Am. Chem. Soc. **113**, 5135 (1991).
[33] Appendix to the report on the International Workshop on Standards and Criteria in Absorption X-Ray Spectroscopy, March 7–9, 1988; Brookhaven National Laboratory, Physica B **158**, 701 (1989).
[34] C. Meneghini, R. Cimino, S. Pascarelli, S. Mobilio, C. Raghu, and D. D. Sarma Phys. Rev. B **56**, 3520 (1997).
[35] S. P. Cramer, in *X-ray Absorption; Principles, Application and Technique*, edited by D. C. Koninsberger and K. Prins (Wiley, New York, 1988), p. 257.